# Diaryliodonium Tetrachloroplatinates(II): Recognition of Trifurcated Metal-involving $\mu_3$-I···(Cl,Cl,Pt) Halogen Bond[†]

Vitalii V. Suslonov,[1] Natalia S. Soldatova,[1,2] Daniil M. Ivanov,[1] Bartomeu Galmés,[3] Antonio Frontera,[3] Giuseppe Resnati[2,4] Pavel S. Postnikov,[2] Vadim Yu. Kukushkin,[1] Nadezhda A. Bokach*[1,2]

[1]*Institute of Chemistry, Saint Petersburg State University, Universitetskaya Nab. 7/9, 199034 Saint Petersburg, Russian Federation*

[2]*Research School of Chemistry and Applied Biomedical Sciences, Tomsk Polytechnic University, Tomsk 634034, Russian Federation*

[3]*Department of Chemistry, Universitat de les Illes Balears, Crta de Valldemossa km 7.5, 07122 Palma de Mallorca (Baleares), Spain*

[4]*NFMLab, Department of Chemistry, Materials and Chemical Engineering "Giulio Natta", Politecnico di Milano, via Mancinelli 7, I-20131 Milano, Italy*

**ORCIDs**

V. V. Suslonov 0000-0002-0769-3992
N. S. Soldatova 0000-0002-1738-4747
D. M. Ivanov 0000-0002-0855-2251
B. Galmés 0000-0001-5975-1317
A. Frontera 0000-0001-7840-2139
G. Resnati 0000-0002-0797-9296
V. Yu. Kukushkin 0000-0002-2253-085X
N. A. Bokach 0000-0001-8692-9627

[†] Electronic Supplementary Information (ESI) available: [Hirshfeld surface analysis, geometric parameters of the discussed contacts, MEP surface of the $[PtCl_4]^{2-}$ anion, experimental data and spectra, crystallographic data]. See DOI: 10.1039/x0xx00000x

## Graphical Abstract

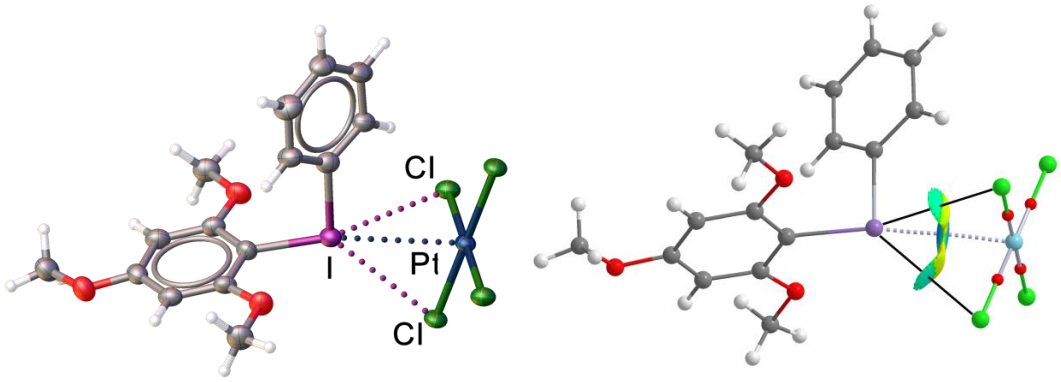


Metal-involving trifurcated four-center $\mu_3$-I···(Cl,Cl,Pt) interaction with iodonium cations, where the positively charged platinum(II) center and two adjacent chloride ligands functioning as an integrated nucleophilic component of the halogen bond.

## Abstract

Synthesis and X-ray characterization of four diaryliodonium tetrachloridoplatinates(II) $[Ar^1Ar^2I]_2[PtCl_4]$ ($Ar^1/Ar^2$ = Ph/Ph **1**, 4-Cl-$C_6H_4$/2,4,6-$(MeO)_3C_6H_2$ **2**, 4-Me-$C_6H_4$/2,4,6-$(MeO)_3C_6H_2$ **3**, Ph/2,4,6-$(MeO)_3C_6H_2$ **4**) allowed to reveal several types of unconventional halogen bonding (HaB) patterns. The first example of metal-involving trifurcated four-center $\mu_3$-X···(X',X',M) HaB is represented by the metal-involving I···Pt HaB (the structure of **4**) with iodonioum cations acting as HaB donors, which is supported by two weak I···Cl HaB contacts. The structures of **1**–**3** display the bifurcated three-center $\mu_2$-I···(Cl,Cl) HaBs with iodonium cations. DFT calculations were used to estimate the energetic features of two types of HaB contacts. ~~by using the quantum theory of "atoms in molecules" (QTAIM) predictor since the interaction energies are dominated by the strong electrostatic attraction between the counterions (ca. −150 kcal/mol). The strength of the directional HaB ranges from −5.5 to −6.8 kcal/mol.~~ Molecular electrostatic potential (MEP) surfaces and the noncovalent interaction plot index

(NCIPlot) computational tools were used to evaluate the σ-holes and characterize HaB, respectively, in all structures.

**Keywords**

Halogen bonding, trifurcate, iodonium(III) species, hypervalent iodine, tetrachloroplatinate(II), DFT

## 1. Introduction

Although halogen bonding (HaB) is a recognized phenomenon since Hassel's Nobel lecture,[1, 2] it was defined by IUPAC only in 2013[3] and in the past decade it has been attracting an increasing attention. This type of noncovalent interaction finds its applications in supramolecular chemistry,[4-10] fabrication of functional materials,[11-14] catalytic transformations and organic synthesis, [15-21] polymer chemistry,[22, 23] drug discovery.[24-27] Importantly, HaB is involved in human physiology.[28, 29] Several highly cited reviews summarize the theoretical and experimental approaches allowing for HaB identification and the numerous areas of application of the interaction.[5, 7, 10, 30-37]

According to IUPAC definition,[3] in a HaB the electrophilic region of a halogen atom (σ-hole, abbreviated as σh) attractively interacts with any nucleophilic region; the electrophilic region is not necessarily electropositive, but it should be less electronegative than the partner. These nucleophilic centers commonly include nonmetals bearing lone pairs, (e.g., O, N, halogen etc.[5]), π-bond(s)[5] systems (e.g., aromatic rings) and, at last, nucleophilic metal centers.[38] Contacts X···M (X = Cl, Br, I; M = any metal) involving *neutral* HaB donors are known for metal centers exhibiting rather strong nucleophilicity, namely $Rh^{I}$,[39, 40] $Ni^{II}$, [41, 42] $Pd^{II}$,[38, 41-45] $Pt^{II}$,[38, 41, 44-48] $Au^{0}$,[49-51] and $Au^{I}$.[52, 53] Most of these metal centers are represented by $d^8$-metals ($Rh^{I}$, $Ni^{II}$, $Pd^{II}$, $Pt^{II}$) bearing a $d_z^2$-orbital which interact with σh ~~(empty σ*-orbital(s))~~ of appropriate HaB donor. Typically HaB donors are iodine-based species such as $I_2$[39, 43] and $R^{EWG}I$.[41, 42] Other halogens featuring a less ~~electrophilic~~ deeper σh, such as Cl[53] and Br,[44, 45] behave as HaB donors toward metal centers significantly more rarely.

The probability of generation of metal-involving HaB and the strength of the interaction can be enhanced by increasing the $d_z^2$-nucleophilicity of the metal center and several ways enable for that. In related recent report by some of us,[48] half-lantern $(Pt^{II})_2$ complexes were employed as metal-based HaB acceptors with increased nucleophilicity. The $d_z^2$-nucleophilicity

enhancement was achieved via the convergence of two metal centers, which are linked through the bridging (thio)azaheterocyclic ligands with rigid geometry. Such convergence of two $Pt^{II}$ centers stimulate repulsive metal–metal interactions between $d_z^2$-orbitals and leads to the increased nucleophilicity of the outer orbitals, which is translated in the formation of a strong HaB with iodine centers of perfluoroiodoarenes.[48]

An alternative approach to the $d_z^2$-nucleophilicity enhancement of a metal center can involve an increase of the electron-donating ability of ligands accompanied by an increase of negative charge on complex; all these phenomena together should provide the electron density drift to metal $d_z^2$-orbitals. Thus, $[PtCl_4]^{2-}$, bearing four σ,π-donating $Cl^-$ ligands and exhibiting the net 2– charge, is a suitable candidate for the search of new metal-involving HaBs. At the same time, the $Cl^-$ ligands themselves can behave as HaB accepting sites, and this increases the possibility of either two-center $\mu_2$-X···Pt and/or multi-center $\mu_n$-X···(Pt–Cl) (n = 2, 3, etc.) HaBs. In this crystal engineering study, we applied diaryliodonium cations as double σh donors having two σh on the extensions of two I–C covalent bonds,[54] thereby determining the increased possibility of forming bi- and trifurcated HaBs.

The present study extends our already reported results on metal-involving HaB[42, 45] and three-center bifurcated HaB.[42] Specifically, in this work we describe the single-crystal X-ray diffraction (XRD) structures of diaryliodonium tetrachloroplatinates (or tetrachloridoplatinate according to the recent IUPAC recommendations[55]) **1**–**4** and we confirm through theoretical calculations the stabilizing nature of the unconventional bifurcated three-center $\mu_2$-I···(Cl,Cl) HaBs and the trifurcated metal-involving $\mu_3$-I···(Cl,Cl,Pt) HaBs observed in the crystal packing of compounds **1**–**3** and **4**, respectively (**Figure 1**, **A** and **C**). The I···Pt contact is the first reported example of metal-involving HaB wherein iodonium cations function as HaB donors.

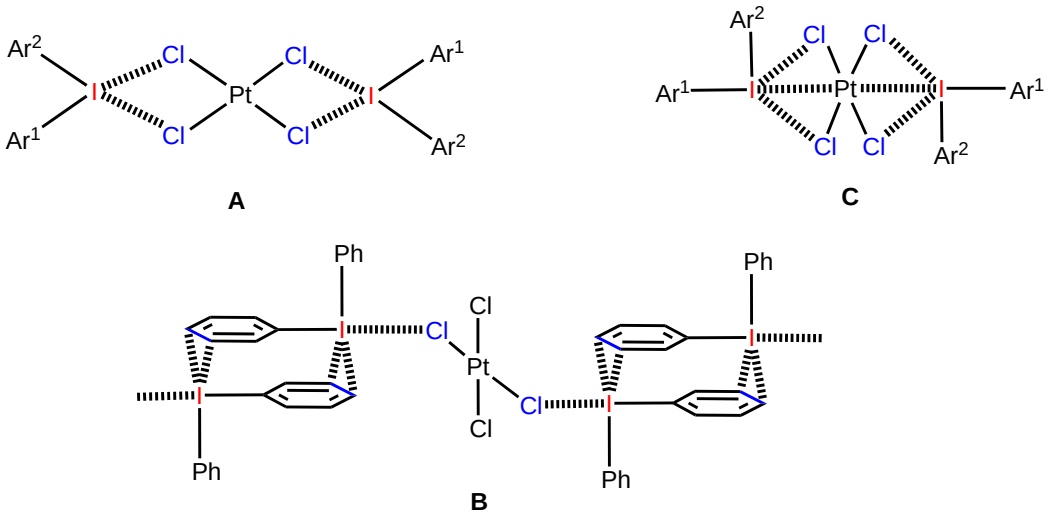


**Figure 1**. Graphical representation of noncovalent binding motifs (dashed lines) observed in crystalline **1**–**4**. Three-center bifurcated $\mu_2$-I···(Cl,Cl) array (A), alternating two-center I···Cl and I···C HaBs (B), and four-center metal-involving trifurcated $\mu_3$-I···(Cl,Cl,Pt) array (C).

## 2. Results and Discussion

**2.1. Synthesis of 1–4 and structural motifs of the XRD structures.** Crystals of compounds **1**–**4**, suitable for single-crystal XRD experiment, were obtained by the treatment of $(Ph_3PCH_2Ph)_2[PtCl_4]$ with $[Ar^1Ar^2I](CF_3CO_2)$ in $MeNO_2$ followed by slow evaporation of the reaction mixtures at room temperature (RT). Iodonium derivatives **2** and **3** co-crystallized with solvent molecules. Compound **2** formed a co-crystal containing two well-defined molecules of nitromethane, while **3** afforded a co-crystal with disordered $MeNO_2$ molecules which were not localized in the packing.

The geometric parameters of $[PtCl_4]^{2-}$ in the structures of **1**–**4** are typical for this dianion[56, 57] and the geometric characteristics of the iodonium cations are comparable to those found in the XRD structures of $[Ph_2I][X]$ (X = $ZnCl_4^{2-}$,[58] $CdCl_4^{2-}$,[58] $Br^-$,[59] $BF_4^-$,[60] $Ts_2N^-$ [61]) and 2,4,6-$(MeO)_3C_6H_4(Ph)I(OAc)$.[62]

In the crystal packing of **1**–**4**, the $[Ar^1Ar^2I]^+$ cations and the $[PtCl_4]^{2-}$ anion act as complementary tectons wherein iodine atoms are involved in two different unconventional supramolecular synthons. The first one was found in the structure of **4** and consists of four-center metal-involving trifurcated $\mu_3$-I···(Cl,Cl,Pt) entity (or, in other words, metal-involving and strong I···Pt linkage supported by two weaker I···Cl interactions), which form neutral trimers (**Figures 1**–**2**).

The second synthon was observed in the structures of **1**–**3** and it consists of three-center $\mu_2$-I···(Cl,Cl) interactions, which form heteromeric trimers $Ar^1Ar^2I^+$–$[PtCl_4]^{2-}$–$Ar^1Ar^2I^+$ (**Figures 1, 3**–**5**). In the case of **2**, such trimers are joined into 1D-chains through Cl···C HaBs formed between the 4-Cl substituent of an iodonium cation and the 3-C atom of the 2,4,6-$(MeO)_3C_6H_2$ ring from another cation. In the structure of **1**, two independent units of $[Ph_2I]^+$ and two halves of $[PtCl_4]^{2-}$ integrate to give two different structural motifs: (i) the trimers formed via the three-center bifurcated contact $\mu_2$-I···(Cl,Cl) considered above; and (ii) an infinite chain assembled via a more conventional two-center I···Cl HaBs, which alternates along the chain with an I···C HaB (**Figure 1**). The latter I···C HaB pairs two iodophenyl rings in an antiparallel geometry.

In the structures of **1**–**4**, independent of the array of observed I···Cl short contacts, chlorine atoms of the $[PtCl_4]^{2-}$ anion, which form the short contacts with iodine, are nearly in the plane formed by iodine and the two covalently bonded carbons. For instance, the distance from the C–I–C plane of the Cl atom that in **1** forms the two-center I···Cl contact is 0.245 Å and the corresponding distances for the chlorine atoms that in **3** form the three-center $\mu_2$-I···(Cl,Cl) interactions are 0.304 or 0.184, respectively. The structure of **4** shows deviation from this general scheme. The separation of Cl1 and Cl2, the two Cl atoms forming the trifurcated $\mu_3$-I···(Cl,Cl,Pt) supramolecular synthon, from the C–I–C plane are 0.307 and 1.880 Å, respectively. The long separation of Cl2 is related to the covalent connectivity in the $[PtCl_4]^{2-}$ dianion and is associated with the longest and weakest HaBs in this four-center system.

The strong electrostatic attraction between the iodonium cation and the tetrachloroplatinate anion plays, no doubt, a role in the formation of I···Cl short contacts, but the coplanarity discussed above clearly proves that also the σhs on iodine play an important role in determining these interactions and their geometry. The observed location of chlorine atoms interacting with iodine is a likely consequence of their tendency to get close to the iodine σhs, which are approximately in the C–I–C plane[52] (**Figure 9**). Indeed, the observed coplanarity can be considered a fingerprint of the HaB component of these interactions, namely a proof that they are charge assisted HaB.

In **sections 2.2–2.3**, we consider the different supramolecular synthons in descending order of their novelty. The unconventional trifurcated metal-involving $\mu_3$-I···(Cl,Cl,Pt) HaB array is discussed first and more common bifurcated three-center $\mu_2$-I···(Cl,Cl) and two-center I···Cl HaBs are considered subsequently. The Hirshfeld surface analysis (HSA)[63-66] gave indications on the relative contribution of all the observed noncovalent forces to the crystal packing of **1**–**4**.

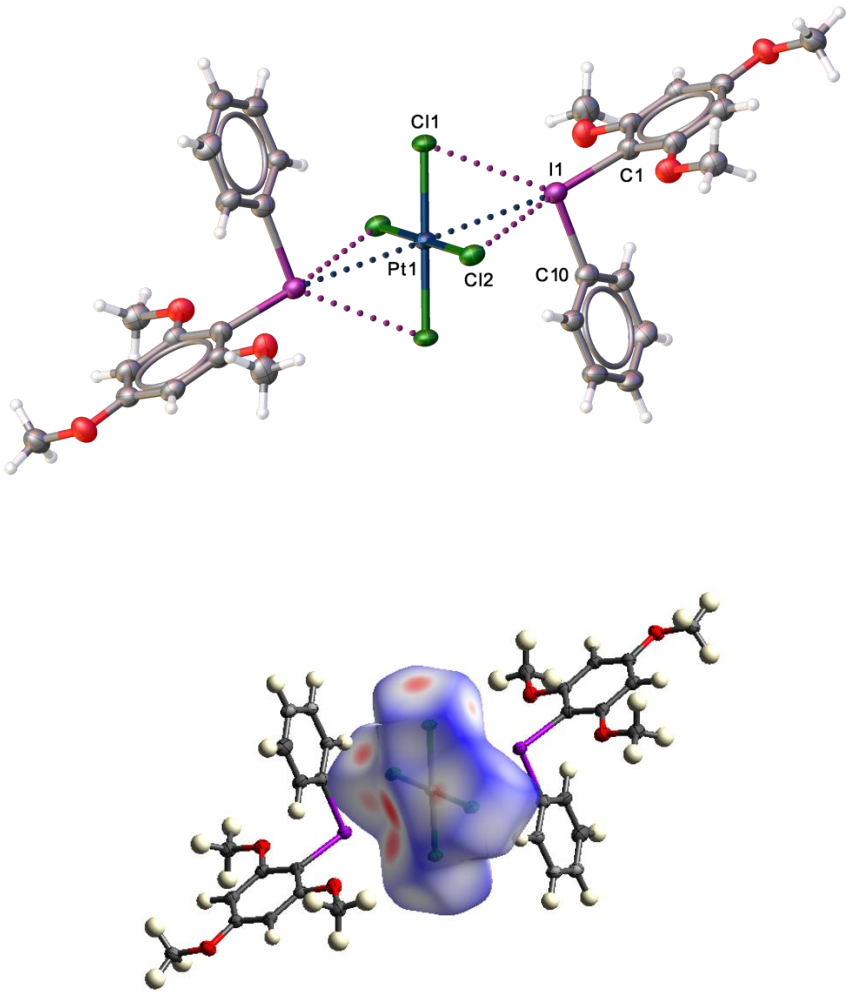


**Figure 2.** Two representations of the trimer present in the crystal of diaryliodonium compound **4**. Top: view evidencing the trifurcated metal-involving $\mu_3$-I···(Cl,Cl,Pt) supramolecular synthon. The contacts shorter than the Bondi vdW sum are given by dotted lines. Thermal ellipsoids are shown with the 50% probability. Bottom: Hirshfeld surface for the $[PtCl_4]^{2-}$ anion in the XRD structure mapped with $d_{norm}$ over the range –0.2070 (red) to 0.9857 (blue).

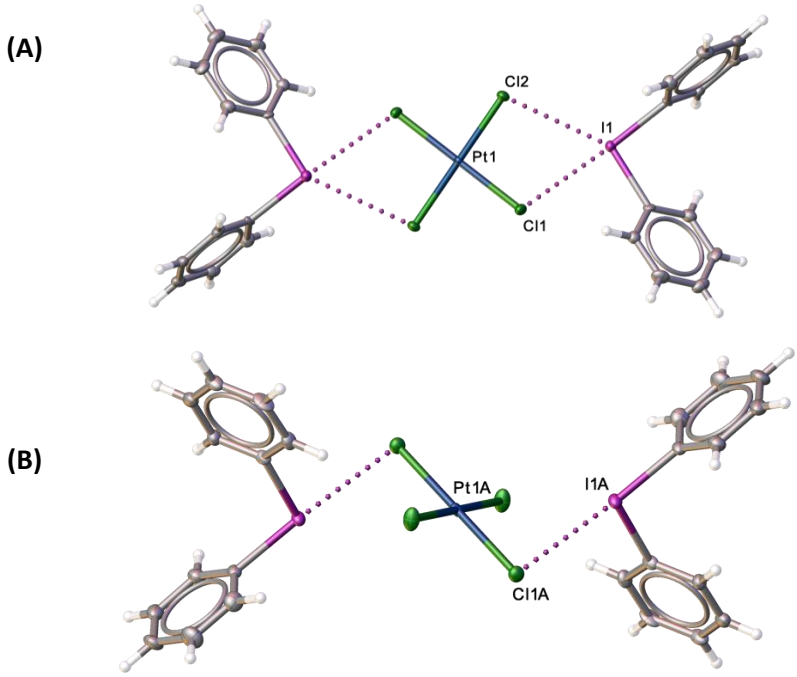


**Figure 3.** Representations of the two HaB based structural units present in the crystal of diaryliodonium compound **1**. Views evidencing the bifurcated three-center $\mu_2$-I···(Cl,Cl) HaB (**A**) and the two-center I···Cl HaB (**B**). The contacts shorter than the Bondi vdW sum are given by dotted lines. Thermal ellipsoids are shown with the 50% probability.

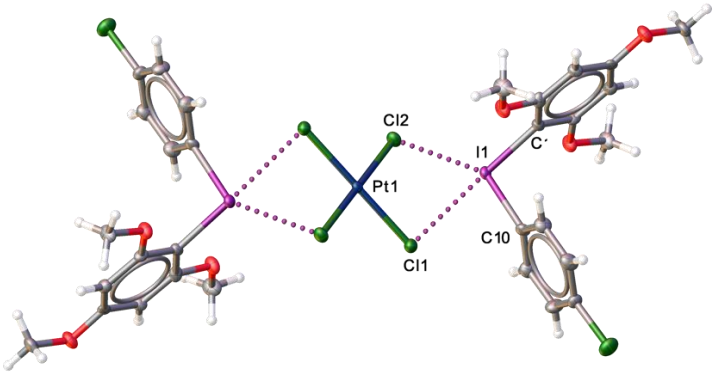


**Figure 4.** Representation of the trimer present in the crystal of diaryliodonium compound **2**, evidencing the three-center $\mu_2$-I···(Cl,Cl) supramolecular synthon. The contacts shorter the sum of Bondi vdW radii are given by dotted lines. Thermal ellipsoids are shown with the 50% probability. ~~Bottom: Hirshfeld surface for the $[PtCl_4]^{2-}$ anion in the XRD structure mapped with $d_{norm}$ over the range −0.3494 (red) to 1.1432 (blue).~~

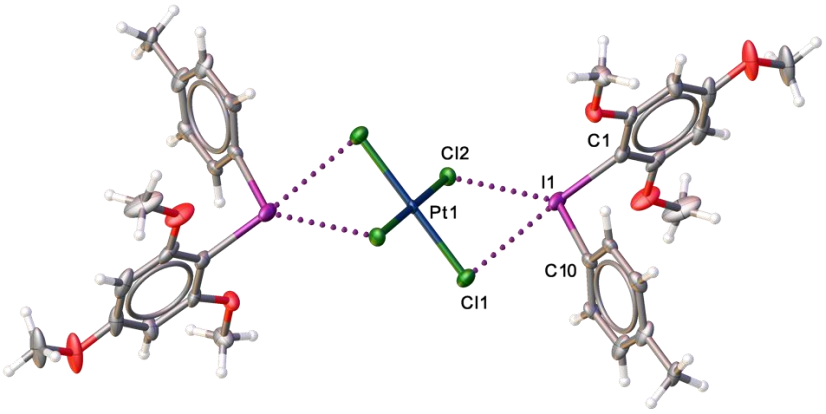


**Figure 5.** Representations of the trimer present in the crystal of diaryliodonium compound **3**, evidencing the three-center $\mu_2$-I···(Cl,Cl) supramolecular synthon. The contacts shorter the Bondi vdW sum are given by dotted lines. Thermal ellipsoids are shown with the 50% probability. ~~Bottom: Hirshfeld surface for the $[PtCl_4]^{2-}$ anion in the XRD structure mapped with $d_{norm}$ over the range −0.3398 (red) to 2.8426 (blue).~~

For all structures, HSA of the $[PtCl_4]^{2-}$ anion (**Figures S1–S4**) indicates the importance of the contacts involving Cl atoms, such as C–H···Cl hydrogen bonding and C–I···Cl charge assisted HaB. Other significant contacts are C–I···Pt and C–H···Pt interactions in **4** and **1**–**3**, respectively.

**2.2. Trifurcated metal-involving $\mu_3$-I···(Cl,Cl,Pt) HaB.** The four-center trifurcated $\mu_3$-I···(Cl,Cl,Pt) supramolecular synthon is a characteristic feature of the structure of **4**. I···Pt and I···Cl separations are 3.3110(3), 3.4520(11), and 3.6005(12) Å long, namely they are shorter than the corresponding Bondi vdW radii sum ($\sum_{vdW}$(I + Cl) = 3.73 and $\sum_{vdW}$(I + Pt) = 3.73 Å; **Table 1**). The geometry of the I···Pt short contact, as indicated by the angles around I and Pt atoms (**Table 1**), safely indicates that the interaction is a metal-involving HaB. Indeed, the ∠(C1–I1···Pt1) is close to linearity (168.52(15)°, namely platinum points to one of the two σh on iodine, while the ∠(I1···Pt1–Cl1) tends to 90° (specifically it is 106.60(3)°), that is to say the I atom sits approximately on the line through Pt and perpendicular to the $[PtCl_4]^{2-}$ plane. Differently, the rationalization of the I···Cl short contacts is less obvious. For the shortest of the

two I···Cl contacts, the values of C1–I1···Cl1 and C10–I1···Cl1 angles are 130.88(16) and 133.47(12)°, respectively, the identification of the σh on the iodonium cation that drives the interaction with chlorine is problematic and the purely electrostatic attraction between the positive iodine and the anion probably plays the major role in determining the short contact. For the longest I···Cl2 contact, the corresponding angles are 148.00(18) and 90.68(14)°. It may seem that the geometry of these two I···Cl interactions makes problematic their rationalization as a HaBs. However, this rationalization appears fully justified considering that the iodine surface featuring two σhs (section 2.4, **Figure 9**) and they tend to form HaBs with the $[PtCl_4]^{2-}$ anion, namely to form short and linear contacts preferentially with its regions of most negative potential. These regions are located along the bisectors of the Cl–Pt–Cl angles rather than on the chlorine atoms (**Figure S5**) and this causes the noticeable deviation from the linearity of the C–I···Cl angles. In other words, the observed I···Cl contacts are the favored arrangement, i.e., the most linear HaBs possible within the constraints of the size and geometry of the polyatomic $[PtCl_4]^{2-}$ anion and its sites of highest electron density. Analogous reasoning may be used to justify the rationalization as HaBs of poorly linear interactions observed in the structures of **1**–**3**.

**Table 1**. Parameters of the trifurcated $\mu_3$-I···(Cl,Cl,Pt) HaB in the crystal of **4**. The color coding for interactions is the same as in **Table 4**; this facilitates correlation between geometric parameters from crystallographic analyses and computational data for any given interaction.

| C–I···X–Y | *d*(I···X), Å | Nc[a] | ∠(C–I···X),° | ∠(I···X–Y),° |
|---|---|---|---|---|
| C1–I1···Pt1–Cl1 | 3.3110(3) | 0.89 [0.80] | 168.52(15) | 106.60(3) |
| C1–I1···Cl1–Pt1 | 3.4520(11) | 0.93 [0.93] | 130.88(16) | 66.80(3) |
| C10–I1···Cl1–Pt1 | | | 133.47(12) | |
| C1–I1···Cl2–Pt1 | 3.6005(12) | 0.97 [0.97] | 148.00(18) | 63.81(3) |
| C10–I1···Cl2–Pt1 | | | 90.68(14) | |

[a]The Normalized contact (Nc) is defined as the ratio between the separation observed in the crystal and the sum of Bondi [or Batsanov[67]] vdW radii of interacting atoms: Nc = d/$\sum_{vdW}$; $\Sigma_{vdW}$(I+Pt) = 3.73 [4.15] Å, $\Sigma_{vdW}$(I+Cl) = 3.73 [3.73] Å.

The structure of **4** represents the first example of metal-involving HaB I···Pt with iodonium cations functioning as HaB donors. $R^{EWG}I\cdots M$ contacts involving *neutral* HaB donors are known, although unusual, and they have been reported for nucleophilic metal centers, namely $Rh^{I}$,[39] $Ni^{II}$,[41, 42] $Pd^{II}$,[38, 41-44] $Pt^{II}$,[38, 41, 46-48] $Au^{0}$,[49-51] and $Au^{I}$,[52] but the I···Pt short contact observed in **4** is the first reported example of metal-involving HaB wherein the HaB donor is an iodonium *cation*. Previous examples of C–I···$Pt^{II}$ noncovalent interactions were found in an Fe-Pt coordination polymer,[41] the complex [Pt(*n*-$C_3F_6$I-3)(Me)(cod)],[68] co-crystals of *trans*-[$PtX_2(NCNR_2)_2$] (X = Cl, Br) with $CHI_3$,[38] [$Pt(acac)_2$]·2(1,3,5-$I_3C_6F_3$),[47] and the co-crystals of the half-lantern complexes [{Pt(C^N)(μ-S^N)}$_2$] (C^N cyclometalated 2-Ph-benzothiazole; S^N 2-SH-substituted *N*-heterocycles) with 1,4-$I_2C_6F_4$ and 1,1'-$I_2$-$C_6F_4$-$C_6F_4$ (**Table S1**).[48] A comparison of I···Pt separations reveals that the I···Pt contact found in **4** is one of the shortest ever observed and, possibly, one of the strongest, probably due to strong electrostatic interaction between the positive iodonium cation and the negative tetrachloroplatinate. Stronger contacts were observed by some of us[48] only in the co-crystals formed with HaB donors by half-lantern $Pt^{II}_2$ complexes, where metal centers exhibit an increased $d_z^2$-nucleophilicity (see Introduction).

The trifurcate binding pattern is a characteristic feature of the μ$_3$-I···(Cl,Cl,Pt) contact. This type of contacts is observed for the first time. Closely relevant known three-center μ$_2$-X···(Cl,Pt) contacts comprise only co-crystals of platinum(II) halide with neutral HaB donors, for instance, *trans*-[$PtCl_2${$NCN(CH_2)_5$}$_2$]·2$CHI_3$,[38] *trans*-[$PtCl_2(NCNMe_2)_2$]·$CHCl_3$·$CBr_4$,[45] and *trans*-[$PtCl_2${$NCNEt_2$}$_2$]·2$CBr_4$.[45] The μ$_3$-I···(Cl,C,Pt) bonding observed in **4** adds to our previous finding[38] showing that the metal-involving trifurcated HaB can be expected when both the metal center and the ligand lone pairs exhibit substantial nucleophilicity, and the two centers are located in closely adjacent positions and function as a single integrated nucleophilic center.

**2.3. Bifurcated three-center $\mu_2$-I···(X,X) HaBs.** *2.3.1. Bifurcated three-center $\mu_2$-I···(Cl,Cl) and two-center I···Cl HaBs in the crystals of **1**–**3**.* Separations between interacting atoms in all charge assisted I···Cl HaBs **1**–**3** are less than the corresponding $\sum_{vdW}$ (**Table 2**).

The structure of **1** contains two independent types of $[Ph_2I]^+$ and of $[PtCl_4]^{2-}$ which afford two different HaB-based supramolecular synthons. They are the three-center bifurcated $\mu_2$-I1···(Cl1,Cl7) HaBs and the more conventional two-center I1A···Cl1A HaB (**Figure 3**, **Table 2**). In addition, I1A forms another weak contact with the π-system of a neighboring $[Ph_2I]^+$ (I1A···C1A 3.496(5) and I1A···C5A 3.507(5) Å). **1** allowed the accurate comparison of $\mu_2$-I···(Cl,Cl) and two-center I···Cl HaBs observed in one structure. In the two-center HaB, the I···Cl distance is shorter than any of the I···Cl distances of the $\mu_2$-I1···(Cl1,Cl7) contact, and the corresponding angle is closer to 180° for the two-center HaB than for the three-center bifurcated $\mu_2$ contacts (**Table 1**, **Figure 6**).

The structures of **2** and **3** display a $\mu_2$-I···(Cl,Cl) pattern similar to that observed in **1**: the four chloride ligands of the tetrachloroplatinate anion form two pairs of HaBs with the iodine atoms of two cations and give rise to a neutral supramolecular trimer (**Figures 4**–**5**, **Table 2**). In the structures of **1**–**3**, each of the $\mu_2$-I···(Cl,Cl) contacts is composed by two inequivalent HaBs (shorter and longer distances are in the range 3.0795(2)–3.1636(11) and 3.3520(3)–3.43021(15) Å, respectively). The strongest bifurcated contact, showing the smallest values for both I···Cl distances, was formed by the $[2,4,6\text{-}(MeO)_3C_6H_4(C_6H_4\text{-}Cl\text{-}4)I]^+$ cation in **2** (**Table 1**). The largest difference between the two distances was observed in the structure of **3** (0.335 Å, **Table 2**), while the smallest difference (0.249 Å) was found for **1**, where the iodonium cation bears two phenyls. The values of the C–I···Cl angles confirm that I atom interacts with two Cl ligands via its two σh.

**Table 2**. Geometrical parameters of C–I···Cl–Pt HaBs. The color scheme is the same as in **Table 4**; this facilitates correlation between geometric parameters from crystallographic analyses and computational data for any given interaction.

| Nos | C–I···Cl–Pt | *d*(I···Cl), Å | ∠(C–I···Cl), ° | ∠(I···Cl–Pt), ° |
|---|---|---|---|---|
| **1** | C1–I1···Cl1–Pt1 | 3.1636(13) | 167.66(10) | 106.21(4) |
| | C7–I1···Cl2–Pt1 | 3.4129(10) | 146.15(13) | 99.26(3) |
| | C1A–I1A···Cl1A–Pt1A | 3.1082(10) | 175.37(13) | 95.12(3) |
| **2** | C1–I1···Cl1–Pt1 | 3.0795(12) | 176.00(13) | 85.45(4) |
| | C10–I1···Cl2–Pt1 | 3.3520(12) | 146.47(14) | 79.29(3) |
| **3** | C1–I1···Cl1–Pt1 | 3.0957(11) | 175.90(12) | 86.83(3) |
| | C10–I1···Cl2–Pt1 | 3.4303(11) | 148.45(10) | 79.13 (3) |
| | | | 139.5(2) | |
| | Reference value[a] | *3.73* | *180* | *90* |

[a]Sum of Bondi vdW radii of interacting atoms ($R_{vdW}$(Cl) + $R_{vdW}$(I)) and angles typical for HaB.

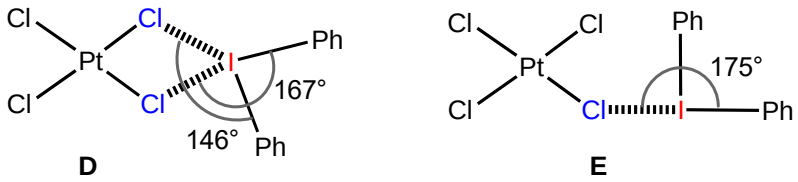


**Figure 6**. Two HaB based supramolecular synthons involving the I atom of the iodonium cations and the chloride ligands of $[PtCl_4]^{2-}$ in the structure of **1**.

*2.3.2. Literature data for bifurcated three-center $\mu_2$-I···(X,X) involving hypervalent iodine(III).* Solid-state structures, where hypervalent iodine(III) functions as a double σh donor toward two-center nucleophiles, are known and include, e.g., the biaxial coordination to iodonium cations of some bidentate *O*,*O*-nucleophiles (diesters and diamides) with 5-atoms (or

higher) spacer between the two HaB accepting centers (**Figure 7**, **F**).[69] This binding pattern was formed also by various adducts given by 18-crown-6 with $[R^1R^2I](BF_4)$ (**Figure 7**, **G**).[70-72] Interestingly, in these structures the biaxial coordination, namely the formation of short contacts, was involving two O atoms separated by the 5-atom of the ($CH_2CH_2OCH_2CH_2$) spacer while the O atom of the spacer affords a more lousy, namely longer, interaction to the area between two σh of the I center.

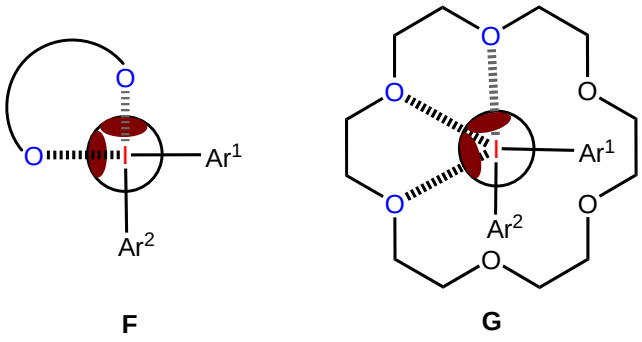


**Figure 7.** Types of known examples of biaxial HaB coordination to hypervalent iodine(III).

The closest analogs of our systems are chelate-like contacts I···(X,X) between iodonium cations and *cis*-$X_2$[M] fragments of the halobismuthates $[Ph_2I]_4[Bi_2X_{10}]$ (X = Br, I).[73] In this system the two I···X interactions and the two C–I covalent bonds affords a nearly square-planar arrangement. We searched and analyzed the Cambridge Structural Database (CSD) for the systems bearing two contacts between the iodine atom of $[R^1R^2I]^+$ and *cis*-$X_2$[A] (A = any atom) moieties and found 67 structures that fulfill these search criteria. Most of them exhibit short contacts between $[R^1R^2I]^+$ cation and a corresponding anion (for instance, $BF_4^-$, $PF_6^-$, $CF_3CO_2^-$, $CF_3SO_3^-$, *p*-$tolSO_3^-$). In these cases, the distance between two nucleophilic centers in the counter-anions (e.g., F···F in $BF_4^-$: 1.95–2.37 Å) is rather small and the proximity of these centers favors the formation of the observed interaction pattern.[74] The bite X···I···X angle in these adducts is in the range 34.3–46.1°, which correspond to the binding of two nucleophilic centers X to one out of two σh of the iodonium cation (**Figure 8**, pattern **H**). Only a few structures feature larger bite angles ∠(X···I···X) in the range 54.9–77.6°; the linkages can be interpreted as

biaxial binding of *cis*-$X_2$-A to both σh of the iodonium cation or as an intermediate case between one σh- and two σh binding (**Figure 8**, patterns **I** and **J**). In both cases it can be anticipated that the electrostatic cation-anion attraction is playing a major role in the short contacts formation.

Parameters for these structures and also those for compounds **1**–**3** are summarized in **Table S2**. Appropriate analysis of contact parameters allowed the attribution of the I···(X,X) contacts to the biaxial binding mode with two σh in iodonium halobismuthates (CSD codes: HAYYIS and HAYZIT) and platinates (**1**–**3**) (**Figure 8**, pattern **I**). The structure of (diketonate)$Eu^{III}$ (CSD code: PUGKIL) features I···(X,X) contacts involving one σh of the iodine (**Figure 8**, pattern **H**) and this geometry is presumably determined by the packing effect and by the steric hindrance of the anion. Similar I···(X,X) contacts involving one σh were identified in iodonium haloaurates (**Figure 8**, pattern **H**); in these salts the other σh of the iodonium cation provides interaction with one more $[AuCl_4]^-$. The structures of iodonium salts of dithiocarbamates (CSD codes: FIFBIF and VATRAJ) can be viewed as an intermediate case, where one nucleophilic center is directed strictly to only one σh of the I center and another nucleophilic center occupies intermediate position between two σhs at one I center (**Figure 8**, pattern **J**). All these results additionally confirm our previous finding that upon interaction with two nucleophilic centers, diaryliodonium cation can exhibit a great variability in values of C–I···X interaction angle,[74] as either contacts with two σhs, one σh, or intermediate geometries can be observed. It is nevertheless useful to observe that consistent with the anisotropic distribution of the electron density on the iodine, namely consistent with the HaB component to the I···X short contacts, the more linear the C–I···X interaction angle is, the smaller the I···X separation is.

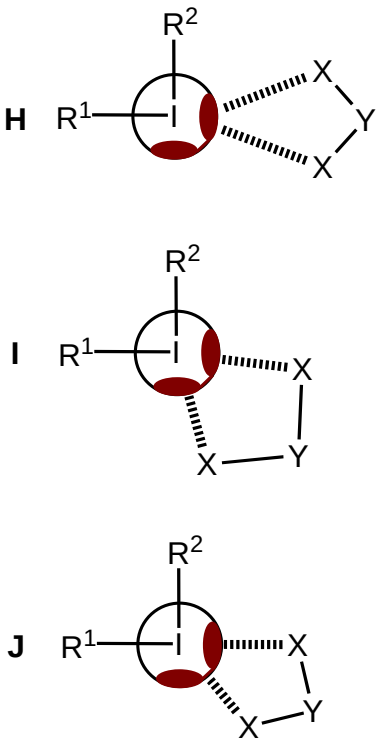


**Figure 8.** Types of $\mu_2$-I···(X,X) contacts in cocrystals of iodonium cations with *cis*-$X_2$[A] moieties.

**2.4. Theoretical calculations.** In order to rationalize the geometric features of the charge assisted HaBs considered above, we carried out a theoretical density functional theory (DFT) study. The molecular electrostatic potential (MEP) surfaces of the cationic parts of salts **1**–**4** are shown in **Figure 9** and the MEP values at the locations labelled as **a**, **b**, and **c** are given in **Table 3**. In all iodonium derivatives two σhs are found on iodine approximately at the extension of the two C–I bonds and the respective electrostatic potentials are different from each other. In compound **1**, both σhs (sites labelled as "**a**" and "**b**") present very similar MEP values and they are more positive than in compounds **2**–**4**. The energy differences at the iodine σhs in these latter derivatives is larger than in **1** and this is mainly due to the fact that the electrostatic potential at the σh opposite to the 4-Cl/Me/H-$C_6H_4$ ring in **2**–**4** is reduced by the overlap of the antibonding C–I σ* orbital with the high electron density associated with the nearby 2,4,6-$(MeO)_3$-$C_6H_2$ π-system (the C–I bond appending the 4-Cl/Me/H-$C_6H_4$ ring to iodine is nearly perpendicular to the 2,4,6-$(MeO)_3C_6H_2$ ring plane, **Figure 9**, bottom panel). It is interesting to observe that due to

the cationic nature of these moieties, the MEP on iodine is positive at any point, even at the location of the two free lone pairs on iodine. The MEP values in between the two σhs (site labeled as "**c**" in **Figure 9**) are also large, thus accounting for a smaller directionality of HaBs in the iodonium cations compared to neutral HaB donors.

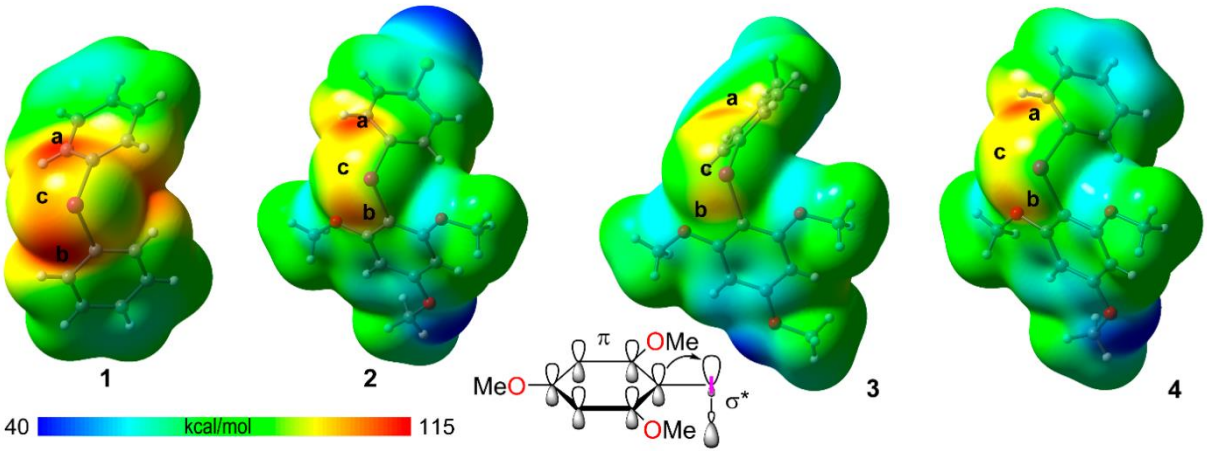


**Figure 9**. MEP surfaces (isosurface 0.001 a.u.) of the iodonium cations in compounds **1** (a), **2** (b), **3** (c) and **4** (d). See **Table 5** for the MEP values at points labelled **a**–**c**.

**Table 3**. MEP values (kcal/mol) at points labelled **a-c** in compounds **1**–**4** (**Figure 9**).

| Compounds | **A** | **B** | **c** |
|---|---|---|---|
| **1** | 115.5 | 112.9 | 102.9 |
| **2** | 109.2 | 102.9 | 95.4 |
| **3** | 102.3 | 96.0 | 87.9 |
| **4** | 108.6 | 99.1 | 91.6 |

The MEP surface of tetrachloroplatinate anion, the common HaB acceptor of compounds **1**–**4**, is shown in **Figure S5**. Its dianionic nature anticipates very large and negative MEP values at any point of the surface. The most electronegative regions are located along the bisectors of the Cl–Pt–Cl angles. The MEP is also large and negative over the center of the Pt–Cl bonds and also over the Pt atom (–190 kcal/mol). In general, the energy differences are small (apart from

that at the extension of the Pt–Cl bonds), thus explaining the variety of geometries observed for the HaB in the structures of **1**–**4**.

We also computed the binding energies of both HaB dimers observed in the crystal structure of **1** (bifurcated three center and two center motifs in **Figure 10**) and performed a QTAIM analysis of critical points (CPs) and bond paths and the NCIplot isosurface. Both dimers exhibit large and similar interaction energies because they are dominated by the electrostatic attraction between the counterions. ~~It thus become quite informative to compare the energetic features of the HaBs by using the QTAIM methodology based on energy predictor. Specifically, we used the potential energy density (Vr) since it has been proved useful to analyze a variety of HaBs.~~[75, 76] The charge density (ρ) and its Laplacian ($\nabla^2\rho$) values associated to structurally relevant HaBs and hydrogen bonds in crystals **1**–**4** are given in **Table 4** and the corresponding bond CPs are labeled in **Figures 10**–**11**. For compound **1**, the QTAIM and NCIplot analyses showed that each HaB in the aggregate formed by the bifurcated three-center $\mu_2$-I···(Cl,Cl) moiety is characterized by one bond CP and bond path interconnecting the I and Cl atoms (**Figure 10**, top). The positive I-atom is located approximately in the plane bisecting the Cl–Pt–Cl bond and perpendicular to the $[PtCl_4]^{2-}$ plane, in good agreement with the MEP surface analysis shown in **Figure 10**. The two HaBs have different geometries and strengths; as expected, the stronger HaB (blue NCIplot isosurface) is also the more directional. ~~The dissociation energies ($E_{dis}$) of the two HaBs are 5.52 and 3.17 kcal/mol, for a total of 8.69 kcal/mol. For the other halogen bonded adduct present in **1**, the $E_{dis}$ of the HaB is 6.34 kcal/mol.~~ Interestingly, a bond CP and a bond path was observed also for another I···Cl contact, (CP labelled as "**d**") that is characterized by a green (*ca*, weak) NCIplot isosurface, consistent with the substantial length of this contact (3.765 Å vs 3.73 vdW sum) and also the smaller values of ρ and $\nabla^2\rho$ at this bond CP compared to CPs labelled "**a**" and "**b**" (**Table 4**). This van der Waals contact can hardly be interpreted as an HaB due to its non-linear geometry (∠(C–I···Cl) 119.83°), long distance and small dissociation energy. This assembly also presents an ancillary hydrogen

bonding that is characterized by a bond CP and bond path connecting the *ortho* C–H bond to one Cl-atom of the anion. ~~, which presents a $E_{dis}$ of 1.22 kcal/mol.~~ This combination of interactions partially explains the greater dimerization energy of this aggregate (–157.0 kcal/mol) with respect to the adduct bonded via the bifurcated three-center $\mu_2$-I···(Cl,Cl) moiety (–152.4 kcal/mol).

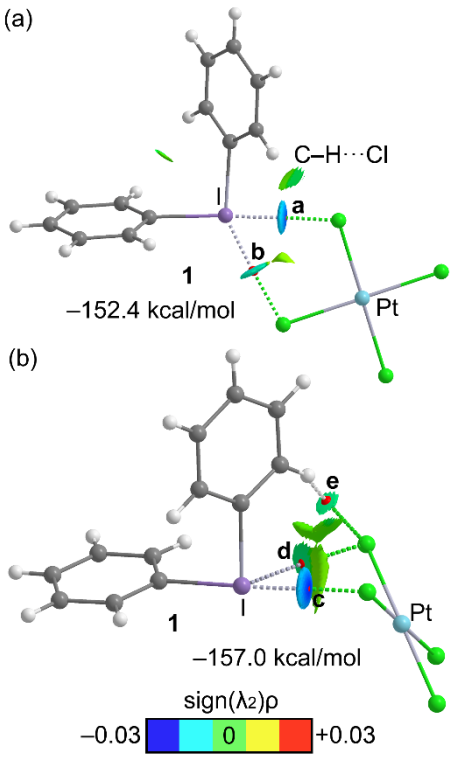


**Figure 10.** Superposition of QTAIM critical points (CPs) and bond paths with the NCIplot surface for the two different halogen bonded adducts present in **1**: HaBs of the bifurcated three-center $\mu_2$-I···(Cl,Cl) moiety (a) and the aggregate formed via the two-center HaB (b). Geometries extracted from the X-ray coordinates. Intermolecular bond CPs are represented using red spheres. The color scale for the NCIplot is −0.03 (blue) < sign($\lambda_2$)$\rho$ < 0.03 (red). Reduce density gradient (RDG) isosurface 0.4. Cut-off for noncovalent contact $\rho$ = 0.04 a.u. Dimerization energies are also indicated.

The HaB dimers analyzed for compounds **2**–**4** are reported in **Figure 11**. The QTAIM analysis shows that here too each HaB is characterized by the corresponding bond CP and bond path interconnecting the I with the Cl or Pt atoms. The analysis also shows the existence of two

ancillary hydrogen bonds in the dimer of compound **4** (**Figure 11**, right). Although no hydrogen bonds are revealed by the QTAIM analysis in the dimers of **2** and **3**, the NCIplot shows the existence of a green isosurface between one aromatic C–H bond and one Cl atom of the dianion, thus suggesting some kind of weak and attractive vdW force. For all compounds, the interaction energies are large and negative, being slightly smaller (in absolute value) in compound **3**, which is the one that presents the smaller MEP values at both σh (**Figure 9**) of the series. Remarkably, the strongest and more directional HaB occurs opposite to the 2,4,6-$(MeO)_3C_6H_2$–$I^+$ bond in very good agreement with the MEP analysis (more positive σh). The binding energy obtained for the dimer of compound **4**, where the C–I bond points directly to the Pt atom, is comparable to those obtained for the dimers of **2** and **3**.

The QTAIM parameters ~~and energies~~ associated to the bond CPs labeled in **Figure 11** are given in **Table 4** and **Table S3**. The strong HaBs (characterized by dark blue NCIPlot isosurfaces) present larger values of ρ and its Laplacian ($\nabla^2\rho$) compared to less directional I···Cl contacts. Moreover, the slightly larger values of all QTAIM parameters (ρ, $\nabla^2\rho$ and Vr and Hr energy densities) obtained for the directional I···Cl HaBs in compounds **2** and **3** compared to the I···Pt HaB in **4**, suggests that the I···Cl HaBs are stronger than the I···Pt HaB. ~~The energies of the strong and directional HaBs (dark blue isosurface) range from 5.52 to 6.68 kcal/mol. The $E_{dis}$ values also demonstrate that the I···Cl HaB is stronger than the I···Pt one (5.52 kcal/mol in **4**). This is partially compensated by the hydrogen bonds (2.36 kcal/mol, CPs **k** and **l**).~~ In complex **4**, the NCIplot index analysis shows the existence of two weak I···Cl contacts as revealed by the green isosurfaces located between the I and two Cl atoms of the tetrachloroplatinate (**Figure 11c**). ~~The energies of the weaker and less directional I···Cl contacts are 3.76 and 3.12 kcal/mol in **2** and **3**, respectively, which are comparable to that of compound **1** (3.17 kcal/mol, CP labelled "**b**" on **Figure 10a**)~~. The total energy density values ($H_r$) given in **Table S3** measured at the bond CPs that characterize the I···Cl HaBs are either positive or very small and negative

revealing the mostly noncovalent nature of the interaction, in line with the positive values of the $\nabla^2\rho$ observed in all bond CPs.

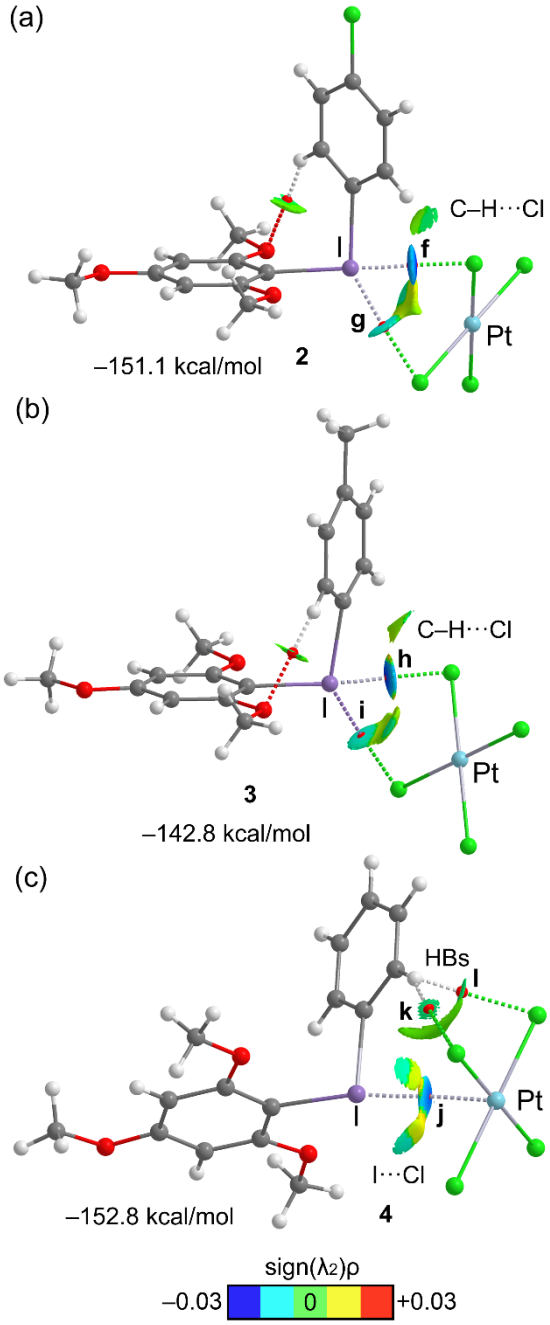


**Figure 11**. Superposition of QTAIM critical points (CPs) and bond paths with the NCIplot surface for compounds **2**–**4**. Geometries extracted from the X-ray coordinates. Intermolecular bond CPs are represented using red spheres. The color scale for the NCIplot is −0.03 (blue) < sign($\lambda_2$)$\rho$ < 0.03 (red). Reduce density gradient (RDG) isosurface 0.4. Cut-off for noncovalent contact $\rho$ = 0.04 a.u. Dimerization energies are also indicated.

**Table 4**. QTAIM Parameters (ρ, and $\nabla^2\rho$ in a.u.) at the bond CP of I···Cl and I···Pt HaBs and H···Cl hydrogen bonds in compounds **1**–**4**. See **Figures 10**–**11** for CP labelling. The color scheme is the same for **Tables 1** and **2** ; this facilitates correlation between geometric parameters from crystallographic analyses and computational data for any given interaction.

| Compound | CP | ρ | $\nabla^2\rho$ |
|---|---|---|---|
| **1** | **a** | 0.0229 | 0.0458 |
| | **b** | 0.0140 | 0.0346 |
| | **c** | 0.0252 | 0.0489 |
| | **d** | 0.0079 | 0.0214 |
| | **e** | 0.0087 | 0.0264 |
| **2** | **f** | 0.0257 | 0.0537 |
| | **g** | 0.0151 | 0.0395 |
| **3** | **h** | 0.0247 | 0.0521 |
| | **i** | 0.0130 | 0.0350 |
| **4** | **j** | 0.0223 | 0.0357 |
| | **k** | 0.0083 | 0.0269 |
| | **l** | 0.0071 | 0.0239 |

## 3. Concluding Remarks

The results from this combined structural and theoretical study can be considered from the following perspectives. In the structure of **4**, we observed the first example of metal-involving trifurcated four-center $\mu_3$-X···(X',X',M) HaB. The metal-involving multi-center HaBs, in which metal center(s) and the adjacent coordinated nonmetal atoms function as an integrated HaB acceptor, are quite uncommon. Up to date, a few examples of computationally proven metal-involving bifurcated three-center $\mu_2$-X···(X',M) HaBs are represented by $\mu_2$-X···(Cl,Pt) (X = Br, I)[38, 45] and $\mu_2$-I···(C,Pt)[48] contacts (**Figure 12**, **K**; M = $Pt^{II}$, X = Cl) and one example of metal-involving tetrafurcated five-center $\mu_4$-I···(Cl,Rh,Cl,Rh) HaB (**M**; M = $Rh^{I}$, X = Cl) has recently been reported by some of us.[40] The five-center HaB (**M**) is transformed to bifurcated three-center $\mu_2$-I···(Rh,Rh) HaB (**N**; M = $Rh^{I}$, X = Cl, Br) when two $\mu_2$-X halide ligands deviate from the plane of the $\{Rh_2X_2\}$ core. Our finding of the trifurcated four-center $\mu_3$-I···(Cl,Cl,Pt) HaB (**L**; M = $Pt^{II}$, X = Cl) fills the gap in the sequence **K**-to-**M** of the known metal-involving multi-center HaBs.

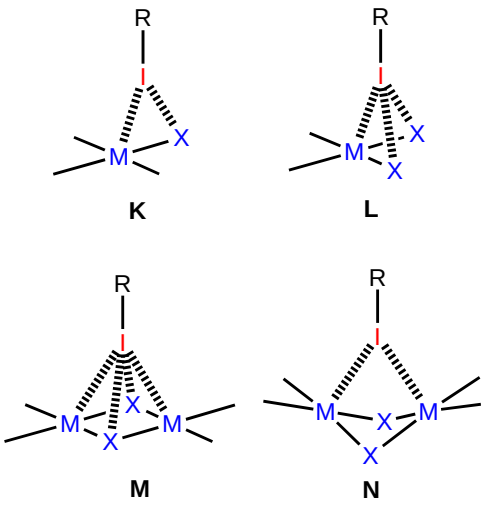


**Figure 12.** Metal-involving multi-center HaBs.

In the structures of **1**–**3**, the bifurcated three-center $\mu_2$-I···(Cl,Cl) HaBs with iodonium cations were identified. Previously it was demonstrated that iodine(III) centers can form three-

center bifurcated HaB with anionic halometallates with $Au^{III}$,[74] and our work provides another example of such contacts. The existence of different HaBs in the structures of **1**–**3** has been confirmed by QTAIM analysis, which shows different bond CPs connecting the I to the Cl atoms. In **2**–**4**, the strongest and directional HaB involves the largest σh that is located opposite to the electron rich π-system due to the electron donation from the π-system to the σh generated by the other π-system. ~~The energy of the I···Pt HaB in **4** is weaker than the I···Cl HaBs in **2**–**3** that is compensated by secondary C–H···Cl hydrogen bonding; the existence of the latter was supported by the QTAIM and NCIplot analyses~~.

This work also demonstrates the potential of $[PtCl_4]^{2-}$ as a square-planar tecton for a supramolecular assembly employing HaBs. The $[PtCl_4]^{2-}$ anion can provide four potential HaB-accepting Cl ligands and one potential HaB-accepting Pt centers. The existence of several HaB-accepting centers leads to different types of $[PtCl_4]^{2-}$-based synthons. In the structures of diaryliodonium tetrachloroplatinates(II), we observed at least three types of HaB-based synthons, e.g trifurcated four-center $\mu_3$-I···(Cl,Cl,Pt), which involve the I···Pt contact with metal, bifurcated three-center $\mu_2$-I···(Cl,Cl), and two-center I···Cl HaB.

In summary, this combined crystallographic and computational study proves that while the energetics of the examined systems is largely determined by the cation-anion attraction, the geometric features of the crystals are strongly affected by the HaBs, consistent with the fact that the directionality is a distinctive feature of this interaction.[5]

## 4. Experimental Section

**4.1. Materials and instrumentation.** The aryliodonium salts $[Ar^1Ar^2I](CF_3CO_2)$[77, 78] and the complex $(Ph_3PCH_2Ph)_2[PtCl_4]$[79] were synthesized accordingly to the published procedures. Other reagents and solvents were obtained from commercial sources and used as received. The HRMS-$ESI^+$ data were obtained on a Bruker micrOTOF spectrometer equipped with

electrospray ionization source; MeOH was used as a solvent. The instrument was operated at positive ion mode using *m/z* range of 50–3000. The capillary voltage of the ion source was set at –4500 V and the capillary exit at (70–150) V. The nebulizer gas pressure was 0.4 bar and drying gas flow 4.0 L/min. Infrared spectra were recorded using a Bruker FTIR TENSOR 27 instrument in KB pellets.

**4.2. Crystallization of $[Ar^1Ar^2I]_2[PtCl_4]$.** A solution of $(Ph_3PCH_2Ph)_2[PtCl_4]$ (5 mg, 4.79 mmol) in $MeNO_2$ (1 mL) was added to a solution of $[Ar^1Ar^2I](CF_3CO_2)$ (5.58 mmol) in $MeNO_2$ (1 mL) and the resulting homogeneous solution was left to stand at RT for slow evaporation for several days. The identity of the crystallized from $MeNO_2$ samples and crystals, studied by single-crystal XRD, is confirmed by the comparison with the powder XRD data (**Figures S13–S14**). Alternatively, **1**–**4** can be obtained from $H_2O$ solutions with almost quantitative yields. For characterization of **1**–**4** see the ESI.

**4.3. X-ray structure determinations.** SC-XRD experiments were carried out using Oxford Diffraction "Xcalibur" and Rigaku "XtaLAB Synergy" diffractometers with monochromated MoKα and CuKα radiation, respectively. The crystals were thermostated at 100 K throughout the all-experiment time. The structures were solved by ShelXT[80] and Superflip[81] structure solution programs using Intrinsic Phasing and Charge Flipping methods, respectively, and refined using ShelXL[80] minimization program incorporated in Olex2[82] program package. The structure 3 contains strongly disordered nitromethane molecule, which was cut out by PLATON[83] Squeeze algorithm. Empirical absorption correction was accounted by CrysAlisPro (Agilent Technologies, 2013) using spherical harmonics, implemented in SCALE3 ABSPACK scaling algorithm. The crystallographic data were deposited in the Cambridge Crystallographic Data Centre under the deposition codes CCDC 2046672–2046675 and can be obtained free of charge via Internet, URL http://www.ccdc.cam.ac.uk/structures/.

**4.4. X-ray powder diffraction.** The powder diffraction experiments were carried out using Rigaku "R-AXIS RAPID II" diffractometer with monochromated CoKα radiation at room

temperature in Gandolfi camera mode. Two-dimensional powder diffraction frames were reduced into standard profiles using osc2xrd[84] program and matched with SC-XRD data using TOPAS 5 (Bruker).

**4.5. Computational details.** The calculations of the monomers and dimers shown in **Figures 10−11** were performed at the DFT level theory using the PBE0[85]-D3[86] method, and the def2-TZVP basis set,[87] with the help of the Turbomole 7.0 software.[88] The topological analysis of the electron density distribution was examined using the quantum theory of atoms in molecules (QTAIM) method developed by Bader[89] and the noncovalent interaction plot (NCIPlot)[90, 91] using the AIMAll program.[92] ~~The estimation of the individual HaB energies was done using the potential energy density ($V_r$) predictor as recently proposed in the literature ($E = 0.778V_r$)[76] for the PBE0 functional.~~ The MEP surfaces were computed at the same level of theory by means of the Gaussian-16 program.[93]

**4.6. Details of the Hirshfeld surface analysis.** HSA was carried out using the CrystalExplorer program.[63-65] The contact distances ($d_i$, $d_e$, and $d_{norm}$),[94] based on Bondi vdW radii,[95, 96] were mapped on the Hirshfeld surface. In the color scale, the negative values of $d_{norm}$ were visualized by red color indicating the contacts shorter than $\Sigma_{vdW}$. The values represented in white denote the intermolecular distances close to the vdW contacts with $d_{norm}$ equal to zero. In turn, the contacts longer than $\Sigma R_{vdW}$ with positive $d_{norm}$ values were colored in blue.

**4.7. Processing of CSD.** Processing of the Cambridge Structure Database (v 5.40) was performed using the ConQuest module (v 2.0.4) and restricted to single crystal structures with determined 3D coordinates and an *R*-factor ≤ 0.1. The analysis for the intra- and intermolecular I···(X,X) interactions was based on two parameters, namely (i) distances $I\cdots X^1$ ($d_1$) and $I\cdots X^2$ ($d_2$), which were restricted by $\sum_{vdW}$[96] (**Figure 13**); (ii) X was restricted to any halogen, chalcogen, and N atoms, Y was any atom, while the $[R^1R^2I]^+$ moiety was positively charged and I atom has only two C-substituents ($R^1$ and $R^2$).

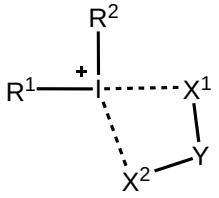


**Figure 13**. Parameters taken for processing of CSD data.

**Acknowledgements**. Support from the Ministry of Science and Higher Education of Russian Federation in framework of "Mega-grant" project (application number 2020-220-08-8827; synthetic studies) is gratefully acknowledged. Authors are much obliged to the Russian Foundation for Basic Research (crystal engineering studies: project 19-33-90059). Physicochemical studies were performed at the Center for X-ray Diffraction Studies, Center for Magnetic Resonance, Center for Chemical Analysis and Materials Research, and Computing Center (all belonging to Saint Petersburg State University). B.G. and A.F., who performed the computational study, thank the MICIU/AEI from Spain for financial support (Project CTQ2017-85821-R, Feder funds).

## References


1. R. S. Mulliken, Structures of Complexes Formed by Halogen Molecules with Aromatic and with Oxygenated Solvents1, *J. Am. Chem. Soc.*, 1950, **72**, 600-608.

2. O. Hassel and J. Hvoslef, The Structure of Bromine 1,4-Dioxanate., *Acta Chem. Scand.*, 1954, **8**, 873-873.

3. G. R. Desiraju, P. S. Ho, L. Kloo, A. C. Legon, R. Marquardt, P. Metrangolo, P. Politzer, G. Resnati and K. Rissanen, Definition of the halogen bond (IUPAC Recommendations 2013), *Pure Appl. Chem.*, 2013, **85**, 1711.

4. L. Brammer, Halogen bonding, chalcogen bonding, pnictogen bonding, tetrel bonding: origins, current status and discussion, *Faraday Discuss.*, 2017, **203**, 485-507.

5. G. Cavallo, P. Metrangolo, R. Milani, T. Pilati, A. Priimagi, G. Resnati and G. Terraneo, The Halogen Bond, *Chem. Rev.*, 2016, **116**, 2478-2601.

6. B. Li, S.-Q. Zang, L.-Y. Wang and T. C. W. Mak, Halogen bonding: A powerful, emerging tool for constructing high-dimensional metal-containing supramolecular networks, *Coord. Chem. Rev.*, 2016, **308**, 1-21.

7. R. Tepper and U. S. Schubert, Halogen Bonding in Solution: Anion Recognition, Templated Self-Assembly, and Organocatalysis, *Angew. Chem. Int. Ed.*, 2018, **57**, 6004-6016.

8. J. Y. C. Lim and P. D. Beer, Sigma-Hole Interactions in Anion Recognition, *Chem*, 2018, **4**, 731-783.

9. S. Scheiner, M. Michalczyk and W. Zierkiewicz, Coordination of anions by noncovalently bonded σ-hole ligands, *Coord. Chem. Rev.*, 2020, **405**, 213136.

10. M. S. Taylor, Anion recognition based on halogen, chalcogen, pnictogen and tetrel bonding, *Coordination Chemistry Reviews*, 2020, **413**, 213270.

11. M. Z. Zhu, C. W. Li, B. Y. Li, J. K. Zhang, Y. Q. Sun, W. S. Guo, Z. M. Zhou, S. P. Pang and Y. F. Yan, Interaction engineering in organic-inorganic hybrid perovskite solar cells, *Mater. Horiz.*, 2020, **7**, 2208-2236.

12. G. Cavallo, A. Abate, M. Rosati, G. Paolo Venuti, T. Pilati, G. Terraneo, G. Resnati and P. Metrangolo, Tuning of Ionic Liquid Crystal Properties by Combining Halogen Bonding and Fluorous Effect, *ChemPlusChem*, 2021, **86**, 469-474.

13. L. Meazza, J. A. Foster, K. Fucke, P. Metrangolo, G. Resnati and J. W. Steed, Halogen-bonding-triggered supramolecular gel formation, *Nature Chemistry*, 2013, **5**, 42-47.

14. F. Meyer and P. Dubois, Halogen bonding at work: recent applications in synthetic chemistry and materials science, *CrystEngComm*, 2013, **15**, 3058-3071.

15. M. Breugst and J. J. Koenig, sigma-Hole Interactions in Catalysis, *Eur. J. Org. Chem.*, 2020, **2020**, 5473-5487.

16. D. Bulfield and S. M. Huber, Halogen Bonding in Organic Synthesis and Organocatalysis, *Chem.-Eur. J.*, 2016, **22**, 14434-14450.

17. S. Benz, A. I. Poblador-Bahamonde, N. Low-Ders and S. Matile, Catalysis with Pnictogen, Chalcogen, and Halogen Bonds, *Angew. Chem. Int. Ed.*, 2018, **57**, 5408-5412.

18. M. Breugst, D. von der Heiden and J. Schmauck, Novel Noncovalent Interactions in Catalysis: A Focus on Halogen, Chalcogen, and Anion-pi Bonding, *Synthesis-Stuttgart*, 2017, **49**, 3224-3236.

19. Y. Wang, J. Wang, G.-X. Li, G. He and G. Chen, Halogen-Bond-Promoted Photoactivation of Perfluoroalkyl Iodides: A Photochemical Protocol for Perfluoroalkylation Reactions, *Organic Letters*, 2017, **19**, 1442-1445.

20. F. Heinen, D. L. Reinhard, E. Engelage and S. M. Huber, A Bidentate Iodine(III)-Based Halogen-Bond Donor as a Powerful Organocatalyst**, *Angewandte Chemie International Edition*, 2021, **60**, 5069-5073.

21. F. Sladojevich, E. McNeill, J. Börgel, S.-L. Zheng and T. Ritter, Condensed-Phase, Halogen-Bonded CF3I and C2F5I Adducts for Perfluoroalkylation Reactions, *Angewandte Chemie International Edition*, 2015, **54**, 3712-3716.

22. G. Berger, J. Soubhye and F. Meyer, Halogen bonding in polymer science: from crystal engineering to functional supramolecular polymers and materials, *Polymer Chem.*, 2015, **6**, 3559-3580.

23. C. G. Wang, A. M. L. Chong, H. M. Pan, J. Sarkar, X. T. Tay and A. Goto, Recent development in halogen-bonding-catalyzed living radical polymerization, *Polymer Chem.*, 2020, **11**, 5559-5571.

24. P. S. Ho, Halogen bonding in medicinal chemistry: from observation to prediction, *Future Med. Chem.*, 2017, **9**, 637-640.

25. A. Pizzi, N. Demitri, G. Terraneo and P. Metrangolo, Halogen bonding at the wet interfaces of an amyloid peptide structure, *CrystEngComm*, 2018, **20**, 5321-5326.

26. C.-M. Hsieh, C.-Y. Chen, J.-W. Chern and N.-L. Chan, Structure of Human Phosphodiesterase 5A1 Complexed with Avanafil Reveals Molecular Basis of Isoform Selectivity and Guidelines for Targeting α-Helix Backbone Oxygen by Halogen Bonding, *Journal of Medicinal Chemistry*, 2020, **63**, 8485-8494.

27. B. Kuhn, E. Gilberg, R. Taylor, J. Cole and O. Korb, How Significant Are Unusual Protein–Ligand Interactions? Insights from Database Mining, *Journal of Medicinal Chemistry*, 2019, **62**, 10441-10455.

28. C. A. Bayse, Halogen bonding from the bonding perspective with considerations for mechanisms of thyroid hormone activation and inhibition, *New J. Chem.*, 2018, **42**, 10623-10632.

29. A. M. S. Riel, R. K. Rowe, E. N. Ho, A.-C. C. Carlsson, A. K. Rappé, O. B. Berryman and P. S. Ho, Hydrogen Bond Enhanced Halogen Bonds: A Synergistic Interaction in Chemistry and Biochemistry, *Acc. Chem. Res.*, 2019, **52**, 2870-2880.

30. D. von der Heiden, A. Vanderkooy and M. Erdelyi, Halogen bonding in solution: NMR spectroscopic approaches, *Coord. Chem. Rev.*, 2020, **407**.

31. H. Wang, W. Z. Wang and W. J. Jin, sigma-Hole Bond vs pi-Hole Bond: A Comparison Based on Halogen Bond, *Chem. Rev.*, 2016, **116**, 5072-5104.

32. M. H. Kolar and P. Hobza, Computer Modeling of Halogen Bonds and Other sigma-Hole Interactions, *Chem. Rev.*, 2016, **116**, 5155-5187.

33. A. Bauza, T. J. Mooibroek and A. Frontera, The Bright Future of Unconventional sigma/-Hole Interactions, *ChemPhysChem*, 2015, **16**, 2496-2517.

34. L. C. Gilday, S. W. Robinson, T. A. Barendt, M. J. Langton, B. R. Mullaney and P. D. Beer, Halogen Bonding in Supramolecular Chemistry, *Chem. Rev.*, 2015, **115**, 7118-7195.

35. A. Mukherjee, S. Tothadi and G. R. Desiraju, Halogen Bonds in Crystal Engineering: Like Hydrogen Bonds yet Different, *Acc. Chem. Res.*, 2014, **47**, 2514-2524.

36. A. Priimagi, G. Cavallo, P. Metrangolo and G. Resnati, The Halogen Bond in the Design of Functional Supramolecular Materials: Recent Advances, *Acc. Chem. Res.*, 2013, **46**, 2686-2695.

37. M. R. Scholfield, C. M. Vander Zanden, M. Carter and P. S. Ho, Halogen bonding (X-bonding): A biological perspective, *Protein Sci.*, 2013, **22**, 139-152.

38. D. M. Ivanov, A. S. Novikov, I. V. Ananyev, Y. V. Kirina and V. Y. Kukushkin, Halogen bonding between metal centers and halocarbons, *Chem. Commun.*, 2016, **52**, 5565-5568.

39. D. W. Shaffer, S. A. Ryken, R. A. Zarkesh and A. F. Heyduk, Ligand Effects on the Oxidative Addition of Halogens to (dpp-nacnacR)Rh(phdi), *Inorg. Chem.*, 2012, **51**, 12122-12131.

40. A. A. Eliseeva, D. M. Ivanov, A. V. Rozhkov, I. V. Ananyev, A. Frontera and V. Y. Kukushkin, Bifurcated Halogen Bonding Involving Two Rhodium(I) Centers as an Integrated σ-Hole Acceptor, *JACS Au*, 2021, DOI: 10.1021/jacsau.1c00012.

41. O. I. Kucheriv, S. I. Shylin, V. Ksenofontov, S. Dechert, M. Haukka, I. O. Fritsky and I. y. A. Gural'skiy, Spin Crossover in Fe(II)–M(II) Cyanoheterobimetallic Frameworks (M = Ni, Pd, Pt) with 2-Substituted Pyrazines, *Inorg. Chem.*, 2016, **55**, 4906-4914.

42. Z. M. Bikbaeva, D. M. Ivanov, A. S. Novikov, I. V. Ananyev, N. A. Bokach and V. Y. Kukushkin, Electrophilic–Nucleophilic Dualism of Nickel(II) toward Ni···I Noncovalent Interactions: Semicoordination of Iodine Centers via Electron Belt and Halogen Bonding via σ-Hole, *Inorg. Chem.*, 2017, **56**, 13562-13578.

43. Y. Yamashina, Y. Kataoka and Y. Ura, Inclusion of an Iodine Molecule in a Tiara-Like Octanuclear Palladium Thiolate Complex, *Eur. J. Inorg. Chem.*, 2014, **2014**, 4073-4078.

44. S. V. Baykov, U. Dabranskaya, D. M. Ivanov, A. S. Novikov and V. P. Boyarskiy, Pt/Pd and I/Br Isostructural Exchange Provides Formation of C–I···Pd, C–Br···Pt, and C–Br···Pd Metal-Involving Halogen Bonding, *Cryst. Growth Des.*, 2018, **18**, 5973-5980.

45. U. Dabranskaya, D. M. Ivanov, A. S. Novikov, Y. V. Matveychuk, N. A. Bokach and V. Y. Kukushkin, Metal-Involving Bifurcated Halogen Bonding C–Br···η2(Cl–Pt), *Cryst. Growth Des.*, 2019, **19**, 1364-1376.

46. R. A. Gossage, A. D. Ryabov, A. L. Spek, D. J. Stufkens, J. A. M. van Beek, R. van Eldik and G. van Koten, Models for the Initial Stages of Oxidative Addition. Synthesis, Characterization, and Mechanistic Investigation of η1-I2 Organometallic "Pincer" Complexes of Platinum. X-ray Crystal Structures of [PtI(C6H3{CH2NMe2}2-2,6)(η1-I2)] and exo-meso-[Pt(η1-I3)(η1-I2)(C6H3{CH2N(t-Bu)Me}2-2,6)], *J. Am. Chem. Soc.*, 1999, **121**, 2488-2497.

47. A. V. Rozhkov, D. M. Ivanov, A. S. Novikov, I. V. Ananyev, N. A. Bokach and V. Y. Kukushkin, Metal-involving halogen bond Ar–I···[dz2PtII] in a platinum acetylacetonate complex, *CrystEngComm*, 2020, **22**, 554-563.

48. E. A. Katlenok, M. Haukka, O. V. Levin, A. Frontera and V. Y. Kukushkin, Supramolecular Assembly of Metal Complexes by (Aryl)I···d [PtII] Halogen Bonds, *Chem.– Eur. J.*, 2020, **26**, 7692-7701.

49. I. Blakey, Z. Merican, L. Rintoul, Y.-M. Chuang, K. S. Jack and A. S. Micallef, Interactions of iodoperfluorobenzene compounds with gold nanoparticles, *Physi. Chem. Chem. Phys.*, 2012, **14**, 3604-3611.

50. Y. Komoto, S. Fujii, K. Hara and M. Kiguchi, Single Molecular Bridging of Au Nanogap Using Aryl Halide Molecules, *J. Phys. Chem. C*, 2013, **117**, 24277-24282.

51. L.-L. Peng, B. Huang, Q. Zou, Z.-W. Hong, J.-F. Zheng, Y. Shao, Z.-J. Niu, X.-S. Zhou, H.-J. Xie and W. Chen, Low Tunneling Decay of Iodine-Terminated Alkane Single-Molecule Junctions, *Nanoscale Res. Lett.*, 2018, **13**, 121.

52. H. M. Yamamoto, J.-I. Yamaura and R. Kato, Multicomponent Molecular Conductors with Supramolecular Assembly: Iodine-Containing Neutral Molecules as Building Blocks, *J. Am. Chem. Soc.*, 1998, **120**, 5905-5913.

53. R.-Y. Liau, H. Ehlich, A. Schier and H. Schmidbaur, Bis(triphenylphosphoranylidene)ammonium Dicyanoaurate(I).*Journal*, 2002, **57**, 1085.

54. G. Cavallo, J. S. Murray, P. Politzer, T. Pilati, M. Ursini and G. Resnati, Halogen bonding in hypervalent iodine and bromine derivatives: halonium salts, *IUCrJ*, 2017, **4**, 411-419.

55. R. M. Hartshorn, K.-H. Hellwich, A. Yerin, T. Damhus and A. T. Hutton, Brief guide to the nomenclature of inorganic chemistry, *Pure Appl. Chem.*, 2015, **87**, 1039-1049.

56. C. J. Adams, M. F. Haddow, R. J. I. Hughes, M. A. Kurawa and A. G. Orpen, Coordination chemistry of platinum and palladium in the solid-state: Synthesis of imidazole and pyrazole complexes, *Dalton Trans.*, 2010, **39**, 3714-3724.

57. D. K. Kumar, A. Das and P. Dastidar, N−H···Cl2−M Synthon as a Structure-Directing Tool: Crystal Structures of Some Perchlorometallates, *Cryst. Growth Des.*, 2006, **6**, 216-223.

58. Y. Wang, I. Fedin, H. Zhang and D. V. Talapin, Direct optical lithography of functional inorganic nanomaterials, *Science*, 2017, **357**, 385-388.

59. T. L. Khotsyanova, T. A. Babushkina, V. V. Saatsazov, T. P. Tolstaya, I. N. Lisichkina and G. K. Semin, Crystal structure and NQR spectra of 79Br, 81Br, 127I diphenyliodonium bromide, *Koord. Khim. (USSR Coord. Chem.)*, 1976, **2**, 1567-1569.

60. Y. T. Struchkov and T. L. Khotsyanova, Crystal structure of diphenyliodonium borfluoride, *Izv. Akad. Nauk SSSR Ser. Khim. (Russ. Chem. Bull.)*, 1960, 821-831.

61. N. Lucchetti, M. Scalone, S. Fantasia and K. Muñiz, Sterically Congested 2,6-Disubstituted Anilines from Direct C−N Bond Formation at an Iodine(III) Center, *Angew. Chem. Int. Ed.*, 2016, **55**, 13335-13339.

62. D. Koseki, E. Aoto, T. Shoji, K. Watanabe, Y. In, Y. Kita and T. Dohi, Efficient N-arylation of azole compounds utilizing selective aryl-transfer TMP-iodonium(III) reagents, *Tetrahedron Lett.*, 2019, **60**, 1281-1286.

63. CrystalExplorer, http://crystalexplorer.scb.uwa.edu.au.

64. C. F. Mackenzie, P. R. Spackman, D. Jayatilaka and M. A. Spackman, CrystalExplorer model energies and energy frameworks: extension to metal coordination compounds, organic salts, solvates and open-shell systems, *IUCrJ*, 2017, **4**, 575-587.

65. M. A. Spackman and D. Jayatilaka, Hirshfeld surface analysis, *CrystEngComm*, 2009, **11**, 19-32.

66. J. J. McKinnon, D. Jayatilaka and M. A. Spackman, Towards quantitative analysis of intermolecular interactions with Hirshfeld surfaces, *Chem. Commun.*, 2007, DOI: 10.1039/B704980C, 3814-3816.

67. S. S. Batsanov, Van der Waals Radii of Elements, *Inorganic Materials*, 2001, **37**, 871-885.

68. L. Xu, D. P. Solowey and D. A. Vicic, Stepwise Conversion of a Platinum Dimethyl Complex to a Perfluorometallacyclobutane Derivative, *Organometallics*, 2015, **34**, 3474-3479.

69. F. Heinen, E. Engelage, C. J. Cramer and S. M. Huber, Hypervalent Iodine(III) Compounds as Biaxial Halogen Bond Donors, *J. Am. Chem. Soc.*, 2020, **142**, 8633-8640.

70. M. Ochiai, T. Suefuji, K. Miyamoto, N. Tada, S. Goto, M. Shiro, S. Sakamoto and K. Yamaguchi, Secondary Hypervalent I(III)···O Interactions: Synthesis and Structure of Hypervalent Complexes of Diphenyl-λ3-iodanes with 18-Crown-6, *J. Am. Chem. Soc.*, 2003, **125**, 769-773.

71. M. Ochiai, K. Miyamoto, T. Suefuji, M. Shiro, S. Sakamoto and K. Yamaguchi, Synthesis and structure of supramolecular complexes between 1-alkynyl(phenyl)(tetrafluoroborato)-λ3-iodanes and 18-crown-6, *Tetrahedron*, 2003, **59**, 10153-10158.

72. M. Ochiai, T. Suefuji, K. Miyamoto and M. Shiro, Effects of Complexation with 18-Crown-6 on the Hypernucleofugality of Phenyl-λ3-iodanyl Groups. Synthesis of Vinyl-λ3-iodane·18-Crown-6 Complex, *Org. Lett.*, 2005, **7**, 2893-2896.

73. Y.-K. Wang, Y.-L. Wu, X.-Y. Lin, D.-H. Wang, W.-T. Zhang, K.-Y. Song, H.-H. Li and Z.-R. Chen, Halobismuthate/diphenyliodonium hybrids stabilized by secondary hypervalent I(III)···X interactions: Structures, optical studies and thermochromisms, *J. Mol. Struct.*, 2018, **1151**, 81-87.

74. I. S. Aliyarova, D. M. Ivanov, N. S. Soldatova, A. S. Novikov, P. S. Postnikov, M. S. Yusubov and V. Y. Kukushkin, Bifurcated Halogen Bonding Involving Diaryliodonium Cations as Iodine(III)-Based Double-σ-Hole Donors, *Cryst. Growth Des.*, 2021, DOI: 10.1021/acs.cgd.0c01463.

75. A. Bauzá and A. Frontera, Halogen and Chalcogen Bond Energies Evaluated Using Electron Density Properties, *ChemPhysChem*, 2020, **21**, 26-31.

76. L. E. Zelenkov, D. M. Ivanov, E. K. Sadykov, N. A. Bokach, B. Galmés, A. Frontera and V. Y. Kukushkin, Semicoordination Bond Breaking and Halogen Bond Making Change the Supramolecular Architecture of Metal-Containing Aggregates, *Cryst. Growth Des.*, 2020, **20**, 6956–6965.

77. N. S. Soldatova, P. S. Postnikov, M. S. Yusubov and T. Wirth, Flow Synthesis of Iodonium Trifluoroacetates through Direct Oxidation of Iodoarenes by Oxone®, *Eur. J. Org. Chem.*, 2019, **2019**, 2081-2088.

78. N. S. Soldatova, P. S. Postnikov, V. V. Suslonov, T. Y. Kissler, D. M. Ivanov, M. S. Yusubov, B. Galmes, A. Frontera and V. Y. Kukushkin, Diaryliodonium as a double sigma-hole donor: the dichotomy of thiocyanate halogen bonding provides divergent solid state arylation by diaryliodonium cations, *Org. Chem. Frontiers*, 2020, **7**, 2230-2242.

79. L. I. Elding, A. Oskarsson, V. Y. Kukushkin and G. K. Anderson, Platinum Complexes Suitable as Precursors for Synthesis in Nonaqueous Solvents, *Inorg. Synth.*, 1996, 276-279.

80. G. Sheldrick, SHELXT - Integrated space-group and crystal-structure determination, *Acta Crystallogr. Sect. A*, 2015, **71**, 3-8.

81. L. Palatinus and G. Chapuis, SUPERFLIP - a computer program for the solution of crystal structures by charge flipping in arbitrary dimensions, *J. Appl. Crystallogr.*, 2007, **40**, 786-790.

82. O. V. Dolomanov, L. J. Bourhis, R. J. Gildea, J. A. K. Howard and H. Puschmann, OLEX2: a complete structure solution, refinement and analysis program, *J. Appl. Crystallogr.*, 2009, **42**, 339-341.

83. A. Spek, PLATON SQUEEZE: a tool for the calculation of the disordered solvent contribution to the calculated structure factors, *Acta Crystallogr. Sect. C*, 2015, **71**, 9-18.

84. S. N. Britvin, D. V. Dolivo-Dobrovolsky and K. M.G., Software for processing the X-ray powder diffraction data obtained from the curved image plate detector of Rigaku RAXIS Rapid II diffractometer, *RMS*, 2017, **146**, 104-107.

85. C. Adamo and V. Barone, Toward reliable density functional methods without adjustable parameters: The PBE0 model, *J. Chem. Phys.*, 1999, **110**, 6158-6170.

86. S. Grimme, J. Antony, S. Ehrlich and H. Krieg, A consistent and accurate ab initio parametrization of density functional dispersion correction (DFT-D) for the 94 elements H-Pu, *J. Chem. Phys.*, 2010, **132**, 154104.

87. F. Weigend, Accurate Coulomb-fitting basis sets for H to Rn, *Phys. Chem. Chem. Phys.*, 2006, **8**, 1057-1065.

88. R. Ahlrichs, M. Bär, M. Häser, H. Horn and C. Kölmel, Electronic structure calculations on workstation computers: The program system turbomole, *Chem. Phys. Lett.*, 1989, **162**, 165-169.

89. R. F. W. Bader, A quantum theory of molecular structure and its applications, *Chem. Rev.*, 1991, **91**, 893-928.

90. E. R. Johnson, S. Keinan, P. Mori-Sánchez, J. Contreras-García, A. J. Cohen and W. Yang, Revealing Noncovalent Interactions, *J. Am. Chem. Soc.*, 2010, **132**, 6498-6506.

91. J. Contreras-García, E. R. Johnson, S. Keinan, R. Chaudret, J.-P. Piquemal, D. N. Beratan and W. Yang, NCIPLOT: A Program for Plotting Noncovalent Interaction Regions, *J. Chem. Theor. Comput.*, 2011, **7**, 625-632.

92. T. A. Keith, AIMAll (Version 19.02.13), 2019.

93. M. J. Frisch, G. W. Trucks, H. B. Schlegel, G. E. Scuseria, M. A. Robb, J. R. Cheeseman, G. Scalmani, V. Barone, G. A. Petersson, H. Nakatsuji, X. Li, M. Caricato, A. V. Marenich, J. Bloino, B. G. Janesko, R. Gomperts, B. Mennucci, H. P. Hratchian, J. V. Ortiz, A. F. Izmaylov, J. L. Sonnenberg, D. Williams-Young, F. Ding, F. Lipparini, F. Egidi, J. Goings, B. Peng, A. Petrone, T. Henderson, D. Ranasinghe, V. G. Zakrzewski, J. Gao, N. Rega, G. Zheng, W. Liang, M. Hada, M. Ehara, K. Toyota, R. Fukuda, J. Hasegawa, M. Ishida, T. Nakajima, Y. Honda, O. Kitao, H. Nakai, T. Vreven, K. Throssell, J. A. Montgomery, Jr., J. E. Peralta, F. Ogliaro, M. J. Bearpark, J. J. Heyd, E. N. Brothers, K. N. Kudin, V. N. Staroverov, T. A. Keith, R. Kobayashi, J. Normand, K. Raghavachari, A. P. Rendell, J. C. Burant, S. S. Iyengar, J. Tomasi, M. Cossi, J. M. Millam, M. Klene, C. Adamo, R. Cammi, J. W. Ochterski, R. L. Martin, K. Morokuma, O. Farkas, J. B. Foresman and D. J. Fox, Gaussian 16, Revision C.01, 2016.

94. J. J. McKinnon, D. Jayatilaka and M. A. Spackman, Towards quantitative analysis of intermolecular interactions with Hirshfeld surfaces, *Chemical Communications*, 2007, DOI: 10.1039/B704980C, 3814-3816.

95. A. Bondi, van der Waals Volumes and Radii of Metals in Covalent Compounds, *J. Phys. Chem.*, 1966, **70**, 3006-3007.

96. A. Bondi, van der Waals Volumes and Radii, *J. Phys. Chem.*, 1964, **68**, 441-451.